Effect of Water Adsorption on Ion Dynamics in Confined Geometry: Na+-Faujasites and Homoionic Alkali Exchanged Montmorillonite

Cyril Abrioux, Sébastien Balme, Benoit Coasne, Sabine Devautour-Vinot, Mohamed Kharroubi, Guillaume Maurin, François Henn

Proc. 3rd Int. Conf. Physics of Solid State Ionics (ICPSSI-3)
J. Phys. Soc. Jpn. **79** (2010) Suppl. A, pp. 19-24

Effect of Water Adsorption on Ion Dynamics in Confined Geometry: Na^+-Faujasites and Homoionic Alkali Exchanged Montmorillonite

Cyril ABRIOUX, Sebastien BALME, Benoit COASNE, Sabine DEVAUTOUR-VINOT, Mohamed. KHARROUBI, Guillaume MAURIN and Francois HENN*

Physicochimie des Matériaux Désordonnés et Poreux, Institut Charles Gerhardt Montpellier, UMR 5253 CNRS, Place Eugène Bataillon, 34095 Montpellier cedex 5, France
(Received November 9, 2009; accepted November 17, 2009)

Various experimental and molecular simulation methods are used to investigate water adsorption and its related effects on ion dynamics in two typical examples of microporous solids: Na^+-Faujasites and homoionic alkali exchanged montmorillonites. Influence of the confinement, of the cationic density and of the cation size is examined. It is then shown that all these parameters play a key role in water adsorption thermodynamics and in the cation/water subsystem dynamics.

KEYWORDS: faujasite, zeolites, montmorillonite, water adsorption, ion dynamics

1. Introduction

Ionic conduction in nanopores is one of the primary "machinery" implicated in life and in many other useful applications in industry as well as in daily life. In the nanoporous solids considered in this work, the so-called extra-framework or exchangeable cations are located at the surface of the nanopores to compensate the negative charge of the framework. The introduction of guest molecules inside the nanopores can modify their position as well as their mobility. Basically, ionic diffusion is low in the dry state and increases when small polar molecules like water, are adsorbed.[1,2,3,4)] It is thus acknowledged that, on the one hand, the ions strongly influence the adsorption of polar molecules and that, on the other hand, the adsorbed molecules permit the ions to diffuse over long distances. However, little is known about the microscopic mechanisms that drive the interplay between the ions and adsorbate molecules in terms of localization and dynamics. In this paper, we will show how the combination of experiments and molecular simulations, yields relevant information about cation dynamics in two Na^+-Faujasite whose the cation density differs and in the whole series of homoionic alkali exchanged M^+-montmorillonite (M=Li,Na,K,Rb & Cs). The effect of water adsorption is investigated by considering dry samples and samples hydrated with various water loadings. Experiments consist of dielectric relaxation spectroscopy (DRS) and thermogravimetric analysis (TGA) measurements. These methods provide insights into ion dynamics and adsorption thermodynamics, i.e. energy barrier for ion hopping and heat of adsorption, respectively. Molecular simulations consist of Monte Carlo (MC) and Molecular Dynamics (MD) simulations. MC simulation allows us to locate the extra-framework cations and the water molecules in the nanoporosity. MD gives the cations and the water molecules displacement and, more specifically in this study, provides information about the possible ionic hop at the surface. Therefore, the coupling of these approaches is shown to provide significant insights into the adsorption mechanism and then into the cation/water molecule subsystem dynamics.

2. Case of the X and Y Faujasites

2.1. forewords

Two Faujasite samples with different Si/Al ratios of 1.0 and 2.4, which correspond to 96 and 56 Na^+ extra-framework cations per unit cell, are considered. In what follows, these two zeolites will be referred to as Na96X and Na56Y, respectively. MC simulations allow us i) to determine the Na^+ location in the dry and hydrated states and ii) to explore the water structure around the cation, i.e. the solvation shell, as a function of the cation location. Furthermore, the comparison of the MC simulation outcomes obtained for the dehydrated state with the activation energy for the localized ionic motion obtained from DRS makes it possible to propose an energy map, named "Ionic Density Of State" (IDOS), which schematically categorizes the cationic sites as a function of their energy level and population. It is then shown that prediction about the water adsorption mechanism, i.e. the subsequent steps of water adsorption, which can be made from IDOS, is in accordance with the data obtained from MC simulation about the cation solvation shell. MD simulation allows us to determine the probability for a cation located in a given site at a time t to move to another site after 2ns, i.e. the final time for each MD run. A comparison of ion dynamics between Na96X and Na56Y is therefore possible.

2.2. Materials

Faujasite is an aluminosilicate zeolite with the general chemical formula $M_{x/m}$, Al_x, Si_{192-x}, O_{384}, where M is the extra-framework cation of charge $+m$.[5)] The number x of cations per unit cell can vary from 0 to 96, depending on the Si/Al ratio. The crystalline structure of Faujasite as well as the position of the extra-framework cations is known from X-ray or neutron diffraction. The faujasite structure contains 192 TO_4 tetrahedra (with T being either Si or Al atom).[6,7)] The alkali extra-framework cations in Faujasite are mainly located in different crystallographic sites that are usually labeled as follows (fig.1): (i) the sites I (SI) are located in the center of the hexagonal prism, while the sites I' (SI') are present in the sodalite cage toward the hexagonal prism, (ii) the sites II (SII) and sites III' (SIII') are located in the 6-ring and 12-ring windows of the supercage respectively, (iii) the sites III (SIII) are in the center of the 4-ring windows of the supercage.

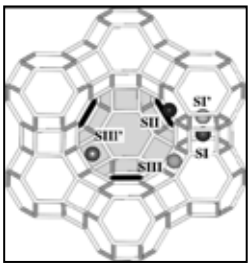

Fig.1: Schematic representation of the Faujasite with the various cationic crystallographic positions. See text for more details about the exact site configuration.

2.3. Methods

2.3.1. Grand Canonical Monte Carlo Simulations (GCMC).

The different structural configurations of Na56Y and Na96X upon various pressure of water were generated using GCMC. All the details about the interatomic potential and the computing procedure are given in previous publications.[8,9)]

2.3.2. Molecular Dynamics (MD).

Starting from the equilibrium configuration obtained from MC simulation, the cation and water molecule dynamics of both Na56Y and Na96X samples were investigated by means of MD simulation. The later was performed using the DLPOLY MD package in the NVT ensemble based on the Berendsen thermostat at 400 K. This temperature is higher than in the MC study, i.e. 300K, in order to observe more significant motion of the cations on a reasonable time scale, i.e. 2ns. The same interatomic potential functions were used in the MD codes as those used in the MC simulations. More details about the computing procedure can be found elsewhere. [9)]

2.3.3. Dielectric Relaxation Spectroscopy (DRS).

DRS is a powerful tool to measure the activation energy associated to the localized hopping of ions in materials such as zeolites. This technique allows one to estimate the cationic population characterizing each cationic sites located at the Faujasite surface (see fig.1). The experimental procedure and the data analysis have been described in details in previous work.[10)]

2.4. Results

2.4.1. Cation location at the dry state.

The comparison between the population of the cations obtained from GCMC simulation[9)] and from DRS[10)] for the two Faujasites in the dry state allows us to ascribe to each cationic site an activation energy (see fig.2, right axis) and a population. Then, assuming that the cations sit in a double potential wells and that the energy level of the transition state is site independent, i.e. the transition state corresponds to a free cation whose energy does not depend on its location, it is shown that the energy level of the cation sitting in its crystallographic site is directly opposite to the activation energy (see fig.2, left axis). The first information that can be extracted from fig.2 is that the extra-framework cations are deeper trapped in NaY than in NaX. The most straightforward explanation for this result is that the higher density of Na^+ in NaX increases the electrostatic repulsion between cations so that their energy level increases.[11)] It can thus be predicted that, in the dry state, Na^+ are likely to be more mobile in Na96X than in Na56Y.

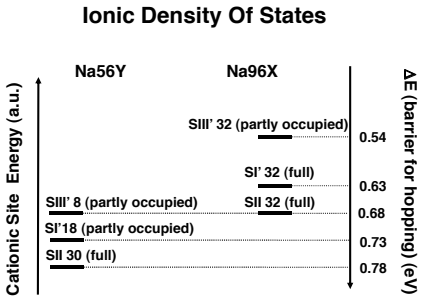

Fig.2: Ionic Density Of States (IDOS) for Na56Y and Na96X. The left axis represents the cationic site energy. The right axis is the experimental activation energy determined from DRS measurements.[10)] Sites occupied by the extra-framework sodium cation are SI' in the sodalite cage, SII and SIII' in the supercage (see fig.1). The number following the cationic site is the site population.

2.4.2. Water adsorption and cation solvation sphere.

Let us first assume that the adsorption of water is favored on cationic sites having higher energy since the cation stabilization by water solvation is larger in that case. IDOS (fig.2) thus provides useful insights into the adsorption mechanism since the adsorption of water molecule is expected to start with the cations of higher energy level. Consequently, we can first predict that Na96X adsorbs the first water molecules more easily than Na56Y and hence that the corresponding water adsorption enthalpy at low coverage is slightly larger for Na96X than for Na56Y. This prediction is in full agreement with the MC simulations and previous gravimetry and microcalorimetry measurements which show that NaX adsorbs more water molecules at low water pressure leading to a higher adsorption enthalpy in NaX.[9,12)] Based on the assumption described above, IDOS also permits to foresee the microscopic mechanism of adsorption, i.e. the successive steps of adsorption on the various cation sites. Once again, the predictions made from IDOS corroborate with the MC calculations regarding the cation solvation upon water adsorption. We report in figs. 3 the number of water molecules that belongs to the first coordination shell of the cation as a function of the water loading for Na96X and Na56Y. This number is determined by the integration of the first peak of the radial distribution function which provides the distance between the center of mass of the water molecule, i.e. the oxygen atom, and that of Na^+ cation. We can then clearly see that the water molecules are first adsorbed on SIII' and SI' cations prior to interact with SII cations as expected from IDOS for both faujasite systems. We also observe that, at high loading, SIII' cations located in the supercage are surrounded by 5 to 6 water molecules. These values are very close to what is found for Na^+ in bulk water.[13)] We can then deduce from these findings that SIII' cations are fully surrounded by water molecules as in the outer-sphere model.[2)] In contrast, SII cations are solvated by a maximum of about 3 water molecules as it can be described by the inner-sphere model.[2)] This outcome cannot be due to confinement only since SII cations are also located in the supercage. Instead, it can be explained from IDOS which predicts that hydration of these cations is less favorable.

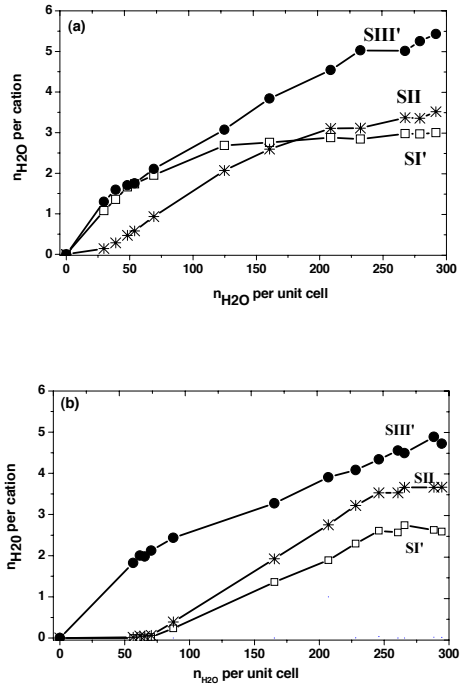

Figs.3. Evolution of the number of water molecules in the first solvation shell of Na^+ as a function of the total number of adsorbed water molecules per unit cell of Faujasite. Na56Y (a); Na96X (b)

Lastly, we note that SI' cations also probably adopt an inner-sphere configuration with only 3 water molecules in their solvation sphere. In that case, however, confinement, due to the much smaller dimension of the sodalite cage in which Na^+ cations are embedded, is likely to be the main reason for this finding. The comparison of results obtained for Na96X and Na56Y shows dissimilarities. Mainly, we observe that SIII' cations are more quickly solvated in the case of Na96X in contrast to SI' cations (figs 3a&b). The reason is that there are more SIII' cations in this sample (see fig.2) to capture the water molecules. Consequently, the water pressure must be higher before the water molecules begin to interact with SI'. Noteworthy, the solvation of SIII' cations at high loadings is a little bit less important in Na96X than is Na56X. This result is likely due to the fact that the same number of water molecules adsorbed in the supercage have to be shared among more cations. Finally, we report in figs.4 the probability calculated from MD simulation for a cation initially located in SII to sit in another site after 2ns. In both systems, we can see that ionic exchange is nearly possible only between SII and SIII' cations which are located in the supercage. In contrast, almost no exchange occurs between these sites and SI'. This behavior is likely due to the fact that the energy barrier that the cations have to overpass for moving from the sodalite to the supercage is too high to make this event observable during the runtime considered in our MD simulations. However, differences between Na56Y and Na96X appear very clearly when considering the ionic exchange between SII and SIII' within the supercage. We observe that, in Na96X, there is no possible exchange at loadings lower than 50 whereas, in Na56Y, SII/SIII' cations exchange appears much more probable. This outcome can be explained by the fact that there are less vacant SIII' in Na96X than in Na56Y (see fig.2), so that cation motion is significantly impeded even in the presence of water molecules.

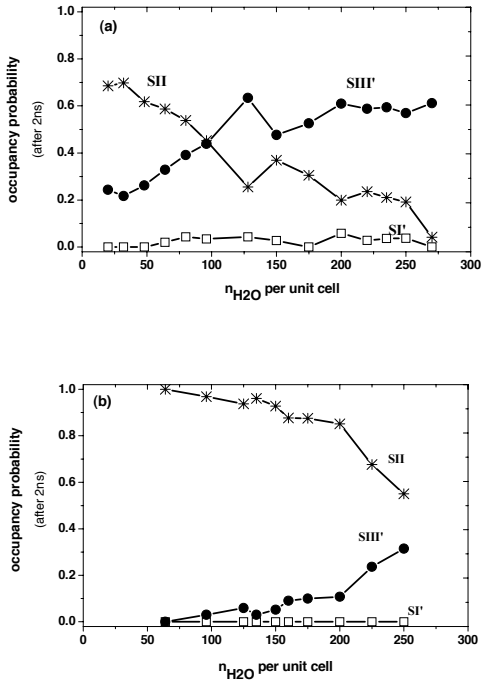

Figs. 4. Probability of finding a cation initially in SII in another site after a given time t. Na56Y (a); Na96X (b)

3. Case of homoionic alkali exchanged montmorillonites

3.1. forewords

As for Faujasite, layered clay minerals as Montmorillonite have exchangeable cations which are located at their inner surface and which are also thought to drive the first steps of water adsorption -or inversely the last steps of water desorption-.[14] In the case of Montmorillonite, the cations which are located in the 2D interlayer space significantly influence the swelling effect resulting from water adsorption.[15] Since cation dynamics, hence dc conductivity, is known to strongly depend on the water loadings, we therefore aim at i) studying dc conductivity of the whole alkali series, i.e. Li^+ to Cs^+, of homoionic montmorillonite as a function of different dehydration states and ii) establishing the connection between dc conductivity and thermodynamics data, i.e. desorption enthalpy. Dc conductivity is measured by means of DRS and its evolution compared to the desorption enthalpies obtained on the same series of samples from TGA and reported in a previous paper.[16] In the case of alkali exchanged Montmorillonite, IDOS cannot be proposed for two reasons. First of all, the exact location of the cation sites is basically not known. Secondly, the adsorption of water, even at low loadings, induced slight modification of the crystallographic structure so that the competition between cation/surface and cation/water interaction energy does not allow us to explain by its own the adsorption energy.

3.2. Materials

The montmorillonite used in this study is supplied by the Clay Minerals Society as source clay

SWy-2-Na-montmorillonite (Wyoming). The homoionic exchange procedure as well as the chemical formula for the whole series of alkali exchanges samples studied in this work will be found elsewhere.[16)]

3.3. Methods

Dc conductivity is extracted from ac conductivity signal recorded at various constant measurement temperatures T in the 10^{-2} Hz to 10^{6} Hz frequency range from a Novocontrol Broad-band Dielectric Spectrometer (BDS 4000). Measurement is performed on pellet obtained by compaction, up to 5 tons, of the considered ≤ 2µm fraction clay powder. A 0.1 µm thick film of Platinum is sputtered on both sides of the pellet in order to ensure a good electrical contact between the sample and the metallic plates of the spectrometer.

Before each measurement, the pellet is dried at 473K for 2 hours and thereafter fully rehydrated in a saturated water vapor atmosphere during 48h at room temperature. The hydrated pellet is then placed into the BDS 4000 cell that is continuously maintained under a dry N_2 flow. The water loading is then obtained by in-situ dehydration during 2 hours at a given Treatment Temperature (TT). After TT , the sample is quickly cooled at about 20 to 30 K.min^{-1} down to 173 K. This modus operandi ensures that the water loading, fixed by TT , is not modified during the "quenching" ramp. The number of water molecules remaining after a given TT has been determined from TGA measurements carried out under the exact same experimental conditions and reported in a previous paper.[16)] TT applied in the present study ranges between 303 and 333K for the various hydrated samples and equals 473K for the dehydrated ones. Depending on the homoionic alkali sample, these values of TT correspond to water loadings comprised between 0 and about 3 to 6 water molecules per alkali cation. These states correspond to the first hydration states for which no swelling is observed. [17,18)] Ac conductivity spectra are first recorded at TT prior to quenching and then at temperatures T comprised between 173K and TT . The Arrhenius plot of dc conductivity, i.e. $\sigma_{dc}.T$ vs T^{-1} can then be plotted.

3.4. Results

3.4.1. dc Conductivity at the dry state

Arrhenius plot of the whole alkali series is reported in fig.5 where it can be seen that dc conductivity strongly depends on the considered alkali sample and that all samples follow the thermal behavior derived from the Nernst-Einstein law:

$$\sigma_{dc} = \frac{\sigma_0}{T}\exp\left(\frac{-\Delta Ea_{\sigma_{dc}}}{k_B T}\right) \qquad (1)$$

where $\Delta Ea_{\sigma_{dc}}$ is the activation energy, σ_0 a pre-exponential factor and k_B the Boltzmann constant. The values of $\Delta Ea_{\sigma_{dc}}$ are 1.08, 0.94, 0.85, 0.82 and 0.8 eV for the Li^+, Na^+, K^+, Rb^+ and Cs^+ montmorillonite respectively. $\Delta Ea_{\sigma_{dc}}$ decreases with the increase of the cation radius, thus indicating that the cation/framework interaction arises mainly from electrostatic forces.

3.4.2. Dc conductivity at various hydrated states

Dc conductivity of all the hydrated samples exhibits a non-Arrhenian behavior. A typical example is given in fig.6. The "1st measurement" point corresponds to dc conductivity measured immediately after TT and before quenching. The "last measurement" point is that obtained after the complete sequence of measurements from 173K to TT .

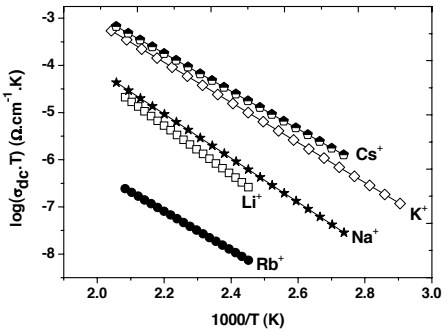

Fig. 5. Arrhenius plot of dc conductivity as a function of the inverse temperature for each homoionic alkali exchanged sample (symbols) and fits (full straight lines) using eq.1.

This temperature evolution is well fitted using the empirical Vogel-Tamman-Fulcher (VTF) law (see fig.6) that is often used for the analysis of dc conductivity in materials as glasses, polymers or melts:[19)]

$$\sigma_{dc} = \frac{\sigma_{0,VTF}}{T}\exp\left(\frac{-\Delta Ea_{\sigma_{dc,VTF}}}{k_B\left(T - T_{VTF}\right)}\right) \qquad (2)$$

where $\Delta Ea_{\sigma_{dc,VTF}}$, $\sigma_{0,VTF}$ and T_{VTF} are the characteristic VTF parameters. If this behavior was due to the departure of water molecules during the course of the experiment, then the Arrhenius plot that could be estimated from the low temperature measurements should match with the first measurement carried out at TT before quenching. As illustrated in fig.6, this is absolutely not the case. Therefore, it seems reasonable to assume that the observed non-Arrhenius behavior is really intrinsic to the sample.

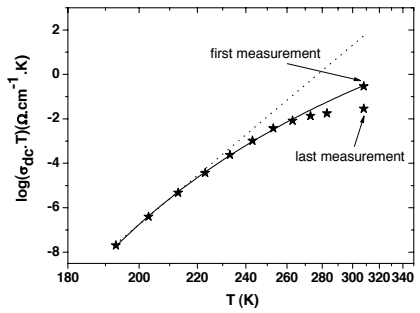

Fig. 6. logarithm of the product dc conductivity.temperature as function of the temperature (in reciprocal scale). Symbols are the experimental data. The dot line is the Arrhenian behavior (eq.1) calculated from the lowest measurement temperatures only. The full line correspond to the VTF fit (eq.2) considering the first measurement and all the measurement comprised between the lowest temperature and $TT - 50K$. See text for more details about the VTF fitting procedure. Case of the Na^+-montmorillonite dehydrated at TT =303K.

The VTF fitting of the data obtained for all the samples at the various dehydrated states allows us to determine the evolution of $\Delta Ea_{\sigma_{dc,VTF}}$ and T_{VTF} with the water loading. It can thus be seen (figs.7) that both parameters continuously deviate from the values characterizing the dry state for which $\Delta Ea_{\sigma_{dc,VTF}} = \Delta Ea_{\sigma_{dc}}$ and T_{VTF} =0 (eq.1). For all samples $\Delta Ea_{\sigma_{dc,VTF}}$ decreases and tends to an asymptotic values of about 0.2 eV. This finding emphasizes that water molecules solvate the extra-framework cations which are thus progressively detrapped from the crystallographic position they occupy at the dry state. It results a decrease in activation energy for ion dynamics and hence for dc conductivity. The asymptotic value of 0.2 eV does not appear to be significantly cation dependent.

The simplest way to explain this behavior is to consider that once the extra-framework cations are solvated by the largest possible number of water molecules, the driving force for dc conductivity becomes related to the displacement of the cation in relation with the monolayer of water molecules and not anymore with the initial cationic sites in which they were embedded. Therefore, the water molecule dynamics turns out to be the key mechanism for ionic conductivity. Similarly to $\Delta Ea_{\sigma_{dc,VTF}}$, T_{VTF} appears to tend to asymptotic values that are, in that case, around 100 K or slightly higher (fig.7b). As T_{VTF} features the departure from the Arrhenius law (eq. 2), the observed behavior means that once a sufficiently high amount of water molecules is absorbed there is no more tremendous change into the sample dc conductivity mechanism. Data reported from Neutron Scattering[20,21,22] or from DRS[23] experiments on fully hydrated samples comparable to ours also reveal the occurrence of an abnormal behavior, i.e. Tg-like of super-cooled water, at temperatures comprised between 100 and 250 K depending on the considered materials. This finding can be associated to non-monotonous temperature dependence of water molecule dynamics resulting from their peculiar environment, i.e. strong interaction with the exchangeable cations and with the rest of the montmorillonite inner surface in the confined geometry constrained by the interlayer nanospace. The exact influence of the cation cannot be unambiguously drawn from the data reported in figs 7. However, it can be underlined that the montmorillonite exchanged with the smallest cations, i.e. Li^+ and Na^+, tend to the asymptotic behavior for lower cation hydration. It would mean that the deviation from the Arrhenius behavior is dependent on the cation radius.

3.4.3. Comparison between thermodynamics of desorption and evolution of dc conductivity

As stated in forewords and then emphasized by the data reported in the previous section, the alkali cations located at the surface of the interlayer space influence the water adsorption and, vice versa, the presence of water molecules in the vicinity of the cations strongly modifies ionic dc conductivity. In order to establish the coupling between water adsorption thermodynamics and dc conductivity in a clearer way, we investigate the variation of the activation energy $\Delta Ea_{\sigma_{dc,VTF}}$ at the hydrated states relatively to the activation energy $\Delta Ea_{\sigma_{dc}}$ measured at the dry state and compared it to the desorption enthalpy. In figure 8, $\Delta(\Delta Ea)$ defined as the difference between $\Delta Ea_{\sigma_{dc,VTF}}(n_{H_2O})$ the activation energy corresponding to n_{H_2O} (fig. 7a) and $\Delta Ea_{\sigma_{dc}}$ the activation energy at the dry state (section 3.4.1) is plotted as a function of the cation radius for different values of n_{H_2O} and compared to ΔH_{desorp} the desorption enthalpy which was estimated from TGA in a previous paper.[16]

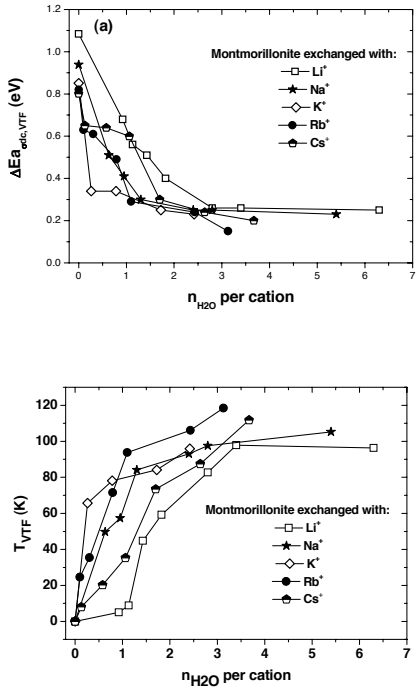

Figs 7: evolution of of $\Delta Ea_{\sigma_{dc,VTF}}$ (a) and T_{VTF} (b) for the whole series of homoionic alkali montmorillonite as a function of the water loadings.

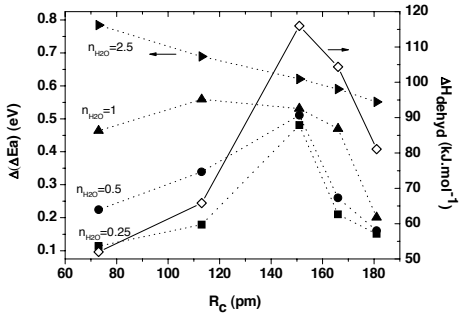

Fig.8 : $\Delta(\Delta Ea)$ (see text for its definition) for various water loadings n_{H_2O} (left axis, symbols !,,,7 & β for n_{H_2O}=0.25; 0.5; 1 & 2.5 respectively) and ΔH_{dehyd}, the dehydration enthalpy, (right axis, symbols M) as a function of the cation radius.

It can then be seen that the cation dependence of $\Delta(\Delta Ea)$ occurs to be akin to that of ΔH_{dehyd} only for the lowest values of n_{H_2O} .This remarkable result undoubtedly

confirms that the very low hydration states are mainly driven by the cation/water interaction and that the depth of the energy wells into which the extra-framework cations are embedded is directly pushed up by the attracting force that the water molecule exerts on the cations. It also indicates that at very low loadings, the cation and its surrounding water molecules probably move together. If not, the activation energy for dc conductivity should also take into account the energy barrier required for breaking the cation/water molecule "bond" and, hence, should be higher than the values measured here.

4. Conclusion

All the data presented in this work emphasize the key role played by the extra-framework cations and their density on the hydration or dehydration of nanoporous aluminosilicates such as zeolites and clay minerals. In the case of the two faujasite zeolites, it is shown that the water molecules are first adsorbed on the sterically accessible cations which sit in surface sites for which the interaction energy with the zeolite framework is the lowest. This finding indicates that water adsorption or desorption is driven by the competition between the cation/surface and cation/water bonding energy. The determination of the cation/framework interaction at the dry state is therefore a pre-requisite for further understanding the earliest stages of water adsorption. Our study also points out that the Ionic Density Of State which can be constructed by coupling DRS experiment and MC simulation is a useful schematic representation. The investigation of both Y and X Faujasites also reveals the influence of the topology on the cation solvation shell. In the largest pore, i.e. supercage, outer-sphere model with 5 to 6 water molecules in the first cation coordination shell is the most likely. In the smaller pore, i.e. sodalite, inner-sphere model with only 2 to 3 water molecules surrounding the cation is the most probable. As a consequence, the fully hydrated cations located in the supercage are much more mobile, thus making possible ionic transport from site to site. This mobility can however be dependent on the cation density and the number of vacant sites. In the case of the whole series of homoionic alkali montmorillonite, IDOS cannot be determined and, hence, a precise knowledge of the adsorption mechanism as that proposed for the Faujasite is much trickier. However, a clear relationship can be established between the activation energy for dc conductivity and its variation as a function of the lowest water loadings with the desorption enthalpy determined by TGA experiments, showing, once again, the privileged role played by the cation on the very low hydration states. Furthermore, this investigation shows an abnormal behavior, i.e. VTF-like, of the cation/water subsystem constrained in the interlayer space. Although the exact origin of this VTF behavior cannot be provided in the light of our data, we note that the critical temperature T_{VTF} tends to asymptotic values close to or higher than 100K (fig.7a) that can be compared to those reported from Neutron Scattering and DRS in similar, though fully hydrated, materials. In the later, the abnormal behavior was ascribed to glassy-type transition of the super-cooled water due to the coupling of the 2D confinement and of the presence of extra-framework cations. Last but not least, this study is a typical example about the fruitfulness of coupling experiments and molecular simulations for getting deeper insights into a complex process, i.e. adsorption phenomenon, in a complex solid state system, i.e. nanoporous aluminosilicates.

1) S. D. Mikhailenko, S. Kaliaguine and E. Ghali: Microporous Mat. **11** (1997) 37.
2) F-R Chou Chang, N. T. Skipper and G. Sposito: Langmuir **11** (1995) 2734.
3) N. J. Garcia and J. C. Bazan: Clay Minerals (2009) 81.
4) E. S. Boek, P. V. Coveney and N. T. Skipper: J. Am. Chem. Soc. **117** (1995) 12608.
5) W. Meier and M. D. H. Olson: *Structure Commission of the International Zeolite Association* (Elsevier: Amsterdam, 1978).
6) A. N. Fitch, H. Jobic and A. Renouprez: J. Phys. Chem. **90** (1986) 1311.
7) G. Vitale, C. F. Mellot, L. M. Bull and A. K. Cheetham: J. Phys. Chem. **101** (1997) 4559.
8) C. Abrioux, B. Coasne, G. Maurin, F. Henn, A. Boutin, A. Di Lella, C. Nieto-Draghi and A. H. Fuchs: Adsorption **14** (2008) 743.
9) C. Abrioux, B. Coasne, G. Maurin, F. Henn, M. Jeffroy and A. Boutin: J. Phys. Chem. C **113** (2009) 10696.
10) A. Nicolas, S. Devautour-Vinot, G. Maurin, J. C. Giuntini and F. Henn: Micro & Mesoporous Mat. **109** (2008) 413.
11) S. Buttefey, A. Boutin, C. Mellot-Draznieks and A. H. Fuchs: J. Phys. Chem. B **105** (2001) 9569.
12) A. Di Lella, N. Desbiens, A. Boutin, I. Demachy, P. Ungerer, J. P. Bellat and A. H. Fuchs: Phys. Chem. Chem. Phys. **8** (2006) 5396.
13) I. J. General, E. K. Asciutto and J. D. Madura: J. Phys. Chem. B **112** (2008) 15417.
14) E. S. Boek, J P.V. Coveney and N.T. Skipper: J. Am. Chem. Soc. **117** (1995) 12608.
15) F. Salles, O. Bildstein, J. M. Douillard, M. Jullien and H. Van Damme: J. Phys. Chem. C **111** (2007) 13170.
16) M. Kharroubi, S. Balme, F. Henn, J. C. Giuntini, H. Belarbi and A. Haouzi: J. Colloid and Interface Science **329** (2009) 339.
17) T. J. Tambach, P. G. Bolhuis, E. J. M. Hensen and B. Smit: Langmuir **22** (2006) 1223.
18) T. Sato, T. Watanabe and R. Otsuka: Clays and Clay Minerals **40** (1992) 103.
19) C. A. Angell, K. L. Ngai, G. B. McKenna, P. F. McMillan and S. W. Martin: J. Appl. Phys. **88** (2000) 3113.
20) J. Swenson, R. Bergman and S. Longeville: J. Chem. Phys. **115** (2001) 11299.
21) F. G. Sanchez, F. Juranyi, T. Gimmi, L. Van Loon, T. Seydel and T. Unruh: J. Phys.:Cond. Mat. **20** (2008) 415102.
22) H. N. Bordallo, L. P. Aldridge, G. J. Churchman, W. P. Gates, M. T. F. Telling, K. Kiefer, P. Fouquet, T. Seydel and S. A Kimber: J. Phys. Chem. C **112** (2008) 13982.
23) L. Frunza, A. Schonhals, S. Frunza, V. I. Parvulescu, B. Cojocaru, D. Carriazo, C. Martin and V. Rives: J. Phys. Chem. A **111** (2007) 5166.